

System for Monitoring Avian Cardiac Output and Breathing Patterns Using Transmission-Type Microwaves

Isao Nakajima^{1*}, Ichiro Kuwahira², Jun-ichi Hata³

Abstract

We report the development of a non-contact monitoring device for avian cardiac output and breathing patterns based on the anterior thoracic air sac pressure that uses transmission-type microwaves (2,400–2,500 MHz, continuous wave). Since the phase waveform represents the dielectric constant change, the phase reflects $-j/\omega\epsilon$ and the dielectric constant change is related to blood flow. The magnitude waveform is reflected from the electronic resistance of tissues due to the expansion of the anterior thoracic air sac, which mainly consists of the thoracic wall. To confirm these waveforms, pigeons and chickens were used for testing. To validate the output waveforms of the developed transmission-type microwave device, data from esophageal catheters and pressure sensors in the anterior thoracic air sac, abdominal air sac, and intraoral cavity were obtained. The waveform for the esophageal catheter, where electrocardiogram electrodes and an angular velocity sensor were installed, correlates with cardiac output. A heart sound microphone was used to confirm the closing sound of the arterial and mitral valves. The experimental results confirm that a linear waveform synchronized with the cardiac blood flow and the anterior thoracic air sac pressure of birds was obtained using transmission-type microwaves. The proposed device, which can monitor cardiac output and respiratory patterns, may enable the early screening of cytokine storms caused by avian influenza viruses. Existing devices use Doppler radar in the 10 to 77 GHz band; these high frequencies are reflected by the chest wall and do not reach deep into body, making it impossible to monitor the blood flow inside the body.

Key Words: Dielectric Constant, Non-Contact, Blood Pressure, Avian Influenza, Screening.

I. BACKGROUND

1.1. Vital Signs

When someone who has caught the flu seeks medical attention, the examining doctor will measure their blood pressure with a sphygmomanometer and listen to their breathing to conduct a pulmonary examination. In mammals and birds infected with the avian influenza virus, the immune system is activated and chemical messengers called cytokines are released from the mast cells of the tissue to fight the virus, increasing the permeability of the vascular wall and allowing amino acids to escape from the blood vessels. A mechanism that facilitates leakage activated. However, when the number of cytokines increases, blood pressure decreases, creating a cytokine storm. In this condition, the lungs become severely edematous and breathing becomes shallow and rapid. For this reason, in humans, the examining physician or nurse monitors blood pressure and observes breathing patterns.

1.2. Related Studies

1.2.1. Radar Doppler Using Microwaves

Several devices for humans based on radar Doppler using continuous waves reflected from the skin of the chest have been developed. Radar Doppler is not limited to medical care; it is also used in health and sleep management. Through vibrations, it can sense whether a person is awake and moving or sleeping. In humans, since the vibration of the heart is transmitted to the chest wall, the heartbeat can be obtained from vibrations of the skin. High-frequency microwaves (10–77 GHz) are reflected at the surface of the body, so the propagation of radio waves is only in the air. The amount of power attenuation is relatively small for this Doppler system, so the microwave transmission power can be very low. However, if the inputs and reflected waves (nonlinear) are simply mixed with each other, the detected signal will be nonlinear waves. To compensate for this shortcoming, a method of simultaneously interfering waves with a phase shift of $\lambda/4$ (λ : wavelength) can be used;

Manuscript received September 14, 2022; Revised October 29, 2022; Accepted November 08, 2022. (ID No. JMIS-22M-10-035)

Corresponding Author (*): Isao Nakajima, +81-90-8850-8380, jh1rnz@aol.com

¹Seisa University, Yokohama, Japan, jh1rnz@aol.com

²Tokai University School of Medicine, Tokyo Hospital, Tokyo, Japan, kuwahira@tok.u-tokai.ac.jp

³Central Institute for Experimental Animals, Kawasaki, Japan, hata@cica.or.jp

however, the improvement is limited. Since it is not possible to obtain waveforms of heart vibrations that hidden under the breathing waves, the frequency peaks (first peak is breathing rate and second peak is heart rate) are obtained by performing the fast Fourier transform (FFT).

Since FFT is an integration of the time axis, the resolution of the time axis is reduced. Therefore, in the RR interval, which requires the accuracy of the time axis, the waveform derived from the heart motion must be extracted, IFFT performed, the original waveform drawn, and the fluctuation of the RR interval must be measured. Since the evaluation of the RR interval is the standard deviation of the interval, accuracy cannot be obtained unless the heart-derived signal is large enough. Regarding radar Doppler, there are no reports on obtaining a blood pressure waveform even if the frequency is lowered to irradiate the inside of the thoracic wall.

1.3. Present Research

Measurement of esophageal impedance for chickens (monitoring of blood pressure and breathing patterns)

We previously developed a device for chickens that can monitor the cardiac output as the phase and breathing changes as the magnitude by adding a 1-MHz medium wave through electrocardiogram electrodes of the esophageal catheter [1-3].

In addition to electrocardiogram electrodes, this avian esophageal catheter incorporates an angular velocity sensor that correlates with stroke volume and a heart sound microphone that can confirm the closing sounds of the aortic and mitral valves.

Based on these physiological data, we can determine the blood flow of the cardiac output and the movement of the thoracic wall associated with respiration. Fig. 1 shows an example of measurement using an esophageal catheter.

Fig. 1 shows (from top to bottom) the invasive axillary artery pressure, magnitude (impedance), angular velocity, electrocardiogram, phase (impedance), and heart sound. The phase waveform shows the outflow from the left ventricle and blood flow into the atria. The closing sounds of the mitral valve and the aortic valve can be confirmed. Since the closing sounds of the aortic valve match the notch timing of the waveform (shape) of the phase, the phase can be determined as the blood flow originating from the heart. Regarding the peak of the axillary artery pressure (measured by invasively cutting down the axillary artery), a propagation delay was observed comparison from the peak of the phase waveform. The difference (L) between heart and axillary artery is the blood flow velocity $V=L/\Delta t$. Our previous paper demonstrates that there is a correlation between the magnitude of the amplitude of the angular velocity and the magnitude of the peak of blood flow [3].

In this paper, a carrier wave of 2.4 GHz is transmitted

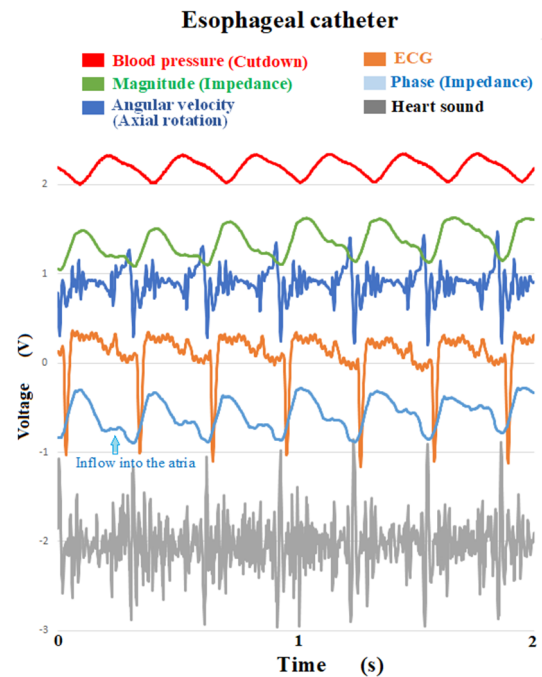


Fig. 1. Esophageal impedance by 1 MHz. Phase is shown in light blue and magnitude is shown in green.

from outside the body, and microwaves that have undergone frequency modulation and amplitude modulation effected by the heart and chest wall, and the phase (frequency) and magnitude (amplitude) are separated and demodulated by the receiving device. Even if the voice is modulated with a medium wave carrier wave on 1 MHz, the voice can be demodulated in the same way even if the voice is modulated with a microwave on 2.4 GHz. Therefore, it is estimated that even if microwaves are used, the impedance waveform will resemble that of 1 MHz of the esophageal catheter. The difference is the site of measurement, that is, the spatial difference. Due to the difference between the measurement-site at a position close to the heart or ribcage and the measurement-site at a distance outside the body, the latter is generally considered to be physically blunted in the waveform. The solution of spatial loss, that could be solved by antenna directivity and penetration of tissue. The longer the wavelength, the better the penetration, and the shorter the wavelength, the sharper the directivity, so there is a spatial gain. These two factors are relationship of tread-off. A practical product for poultry farmers to understand the health status of their birds must be contactless. Because chickens are handled in cages. With this in mind, this paper describes the method and results of how to find the trend-off conflict.

1.4. Multimedia Data Analysis is Essential

The circulation and respiratory monitoring using with microwave are methods that do not contact the individual, and are spatially separated from the heart, lungs, and air

sacs. So what does the microwave waveform mean? Is the temporal timing consistent with other multimedia data? These points must be watched. Occasionally, it may be observed with delays or skeletal muscle spasms as a noise. In order to evaluate, multimedia data measured in multiple dimensions, are essential. The further the distance from the heart, the more supplementary correction data is required. Therefore, the evaluation of microwave waveforms shall be recommended with data analysis by multimedia.

1.5. Noise Also Has Meaning in Birds without a Diaphragm

Birds do not have a diaphragm, so skeletal muscles in the abdomen and chest control balloons called air sacs to direct airflow into the lungs. Avian lungs are hard, and in addition to ventilation, which draws in outside air through the trachea, airflow is also exchanged between air sacs. Therefore, airflow flows into the lungs multiple times in one ventilation. Skeletal muscles are always in a state of tension, which suggests that the sympathetic nerves, which control the excitation state of skeletal muscles, maintain a dominant state in the autonomic nerves. The bar-tailed godwits tacked by GPS, a migratory bird that flies for 14 days without rest and sleep, flying from Alaska to the off-shore of New Zealand [28]. It is extremely difficult for humans, mammals, to run a marathon 24 hours a day, but birds have a physiological structure that allows them to maintain sympathetic excitation at all times. Therefore, in respiratory monitoring, skeletal muscle spasm may appear in the air sac pressure, but this is not noise but important information controlling the flow of air between air sacs. Therefore, air sac pressure monitors must be amplified even at relatively high frequencies without noise rejection.

II. PRINCIPLE

2.1. Free-Space Propagation Loss

Here, we explain the principle of monitoring the blood flow associated with the heartbeat and the breathing pattern associated with the movement of the thorax. The relationship between the free-space propagation loss and frequency can be expressed as

$$\text{Loss(dB)}=20 \times \log\left(4 \times \pi \times \frac{R}{\lambda}\right) .$$

$$\lambda = \frac{c}{f}$$

c: speed of light (m/s)

f: frequency (Hz)

R: distance (m)

λ: wavelength (m)

From this equation, the attenuation is 29.77 dB at 2,450 MHz and a distance of 30 cm.

2.2. Half-Power Depth

The proposed device passes microwaves through the bird's tissue and measures changes in impedance. The tissue attenuates the microwave power. Under the assumption that the depth at which power is attenuated by half is *D*, the relationship between frequency *f*, dielectric constant ϵ_r , and the dielectric dissipation factor ($\tan \delta$) is as follows.

$$D = \frac{3.31 \times 10^7}{f \times \tan \delta \times \sqrt{\epsilon_r}} \quad 0 \leq \delta \leq \pi.$$

The dielectric loss tangent is a numerical value that expresses one aspect of the ratio at which part of the energy becomes heat when an AC electric field is applied to a dielectric. If an AC electric field is applied to an ideal dielectric and only the capacitance component (capacitor) is considered, there is a 90-degree phase difference between the electric field and the current due to polarization/charge reversal.

The power consumption of the AC current is expressed as the vector product of the electric field and the current, so if the phase difference between the two is 90 degrees, the power consumption will be zero. It becomes an ideal dielectric. However, in actual materials, complete insulation is not possible. The resistance of the dielectric itself is finite, so a leakage current is generated. In addition, dielectric polarization and partial discharge create a parallel resistance component. The phase difference is thus shifted from 90 degrees. Let δ denote the shift from 90 degrees. Its tangent ($\tan \delta$), called the dielectric tangent, corresponds to the component where the electric field and current are in phase. Only this in-phase component contributes to power consumption or loss. The dielectric loss tangent is proportional to the dielectric loss [4-13]. In addition, the complex dielectric constant due to the parallel plate capacitor due to the difference in materials is described in the literature [14], the difference in the frequency characteristics of pure water and blood is described in [15], and the effects of weak microwave exposure are described in [16].

The dielectric constant of water is about 80. In living organisms, glucose in body fluids decreases the dielectric constant. Under the assumption that a body fluid has an average glucose content of 5%, the dielectric constant is 76.5 at around 2,450 MHz, as shown in Fig. 2.

Furthermore, the non-dielectric constant of the chest is lowered by the air in the lungs, connective tissue fibers, fatty tissue, etc., so the average non-dielectric constant can be considered to be 25.5 or lower. For the estimation of the attenuation of microwaves, a factor of 25.5 may be chosen to maximize attenuation.

From Fig. 3, the power half-power depth is 26.2 mm with a non-dielectric constant of 25.5, so it is 4 times this (2 to the power of 4=16) 26.2×4=104.8 mm Approximately 105

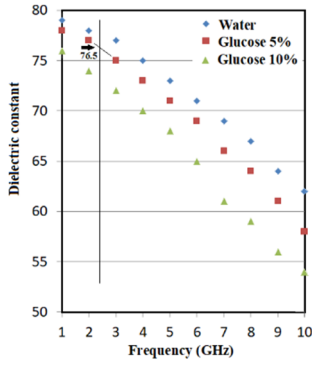


Fig. 2. Glucose concentration and dielectric constant.

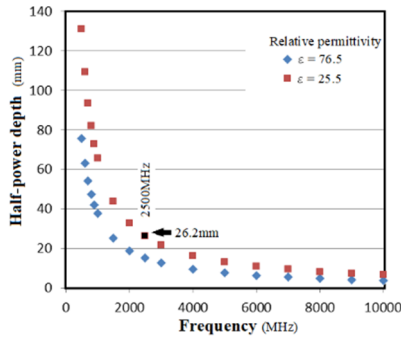


Fig. 3. Half-power depth versus frequency for dielectric constants of 76.5 and 25.5.

mm has 1/16 of the power. The power is attenuated by -12 dB corresponds to half-power loss (1/16=-12 dB). It is assumed here that 105 mm is approximately the width of the anterior chest of a large chicken.

2.3. Scattering Loss

For microwaves, a higher frequency leads to more energy being reflected by the surface of a substance. Less energy is reflected when the wave is incident at right angles to the surface. Whether the reflective surface of an uneven material can be regarded as flat is determined by the Rayleigh roughness criterion, expressed as

$$g=4\pi\sigma/\lambda\sin \theta,$$

where σ is the standard deviation of the undulation amount in the first Fresnel zone and θ is the incident angle with respect to the normal direction of the surface.

If $g < 1$, the reflective surface is flat; if $g > 1$, it is undulating. In chickens and pigeons, the probe is placed perpendicular to the chest wall.

Since the wavelength for 2.5 GHz waves is 12 cm and a bird's skin is smooth, $g < 1$. In experiments with chickens and pigeons, the probe was intentionally set perpendicular to the chest wall, with a wavelength of λ 12 cm at a frequency of 2.5 GHz. Since the denominator of the above

formula is large enough, the skin of birds is smooth, and $g < 1$ is self-evident. There is no problem numerically assuming that scattered waves are relatively small at 2.5 GHz. However, the beam half width of the 10 dBi antenna is 49 degrees, so the scatter increases geometrically (it is not a pointing loss). Based on the past propagation experiments at 2.5 GHz show that the beam direction of antenna is incident perpendicularly (almost 90 degrees) and reflected or scattered by the skin, resulting in a halving of the power (i.e., a 3 dB drop).

2.4. Equivalent Circuit

In the equivalent circuit of avian thorax, R_{body} is the change in distance mainly due to the movement of the ribcage. This change is very large. Many radar Doppler systems track only real numbers and blood flow cannot be seen logically because they calculated only magnitude (real number). Even if the change in blood flow is reflected in the real number ΔR , a small ΔR cannot be detected unless the dynamic range of the radar Doppler system is increased and the amplification circuit is not linear. The amount of change in blood flow on the real axis ($R_{leakage}$ in Fig. 4) is about 1/100 of the resistance value of the thorax.

In addition, the notch caused by the aortic valve closure cannot be seen in the real axis direction change unless the resolution is high. Previous studies have thus applied the FFT power spectrum to the received waveform. The first peak is taken as the respiratory rate and the second peak is taken as the heart rate.

In birds, the heart is covered by a large sternum and thus the vibrations of the heart are only slightly transmitted to the skin. The valve closing sound is even difficult to detect using a stethoscope. Reflective microwave radar, which detects skin vibrations, thus cannot be used for birds.

Using the equivalent circuit shown in Fig. 4, it is possible to measure the change on the complex plane, where the imaginary part is the phase and the change in the real number is the magnitude, using transmission-type microwaves (continuous waves), as described later.

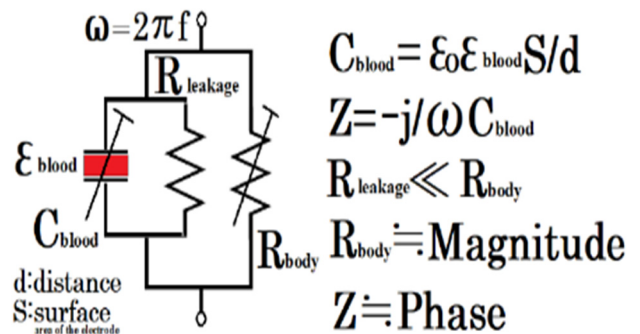


Fig. 4. Equivalent circuit of avian thorax.

2.5 Circuit Design

Specifically, when the transmit and receive antenna gains are 10 dBi, the frequency is 2,450 MHz, and the distance is 30 cm, the transmit power is -40 dBW and the received power is -67.76 dBW. The theoretical margin is 40.75 dB. Such a margin is difficult to obtain with radar Doppler.

Chickens are constantly moving and thus there is a pointing loss of the antenna toward the heart. In addition, the skeletal muscles of chickens constantly vibrate to control skeletal muscles which keep tension of air sacs [2], and those vibration causes fluctuations in the baseline of noise level. The actual measurement margin is about 30 dB, which is different from the theoretical value, but this 30 dB margin is necessary to draw the phase waveform including the notch of the aortic valve. Table 1 shows the line design of the system considering the free-space propagation loss, half-power depth, reflection/scattering, and pointing loss.

III. METHODS

3.1. Verification Experiment

The conceptual diagram and block diagram of the implemented system are shown in Fig. 5. The reflection coefficient (S_{11}) of the antenna built into the probe is shown in Fig. 6. The implemented device is shown in Fig. 7. The experimental conditions are summarized in Table 2.

3.2. Insertion of Auxiliary Sensor

It is necessary to measure the heart and respiration with another sensor to corroborate the microwave measurements. In pigeons, an air pressure sensor and an electrocardiogram electrode were surgically sewn subcutaneously in the sagittal direction in the midline of the back under isoflurane inhalation anesthesia in advance. The implemented

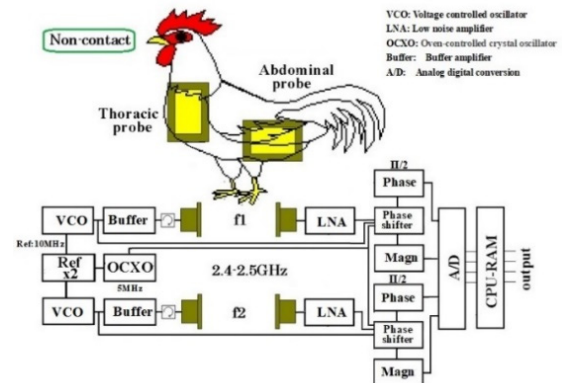


Fig. 5. Conceptual and block diagrams of implemented system (f1 and f2 are 2,400–2,500 MHz ISM band continuous waves).



Fig. 6. The reflection S_{11} parameter of antenna in probe. The antenna is adjusted so that the dip comes to the frequency of 2.4 GHz.



Fig. 7. Implemented transmission-type microwave device for pigeons (chest antenna: horizontal polarization, abdomen antenna: vertical polarization).

Table 1. Circuit design (theoretical values).

Target birds	5 pigeons (weight 450–470 g)	8 chickens (weight 1,000–2,500 g)
Frequency/ output	2,400–2,500 MHz–40 dW	2,400–2,500 MHz–40 dW
Distance be- tween probes	20 cm	30 cm
AD conversion	6 bits, quantization 500 /sec. or ,2,000 /sec	6 bits, quantization 500 /sec. or 2,000/ sec.
Measurement state	Inhalation anesthesia or no anesthesia	Inhalation anesthesia or no anesthesia
Signal detection	Amplitude synchronous detection (obtain two orthogonal signals with PSN)	Amplitude synchronous detection (obtain two orthogonal signals with PSN)

transmission-type microwave device for pigeons (chest antenna: horizontal polarization, abdomen antenna: vertical polarization) is shown in Fig. 7.

For chickens, an esophageal catheter can be inserted through the crop to the side of the heart. While maintaining inhalation anesthesia and spontaneous breathing, the operator guided the esophageal catheter to pass through the crop and into the lower esophagus. Isoflurane was then discontinued, sufficient air was aspirated, and the chicken was gently aroused and kept upright for the transmission-type microwave examination and data acquisition. The esophageal catheter was removed when it was noticed by the chicken. Data were then collected continuously. In addition, pressure sensors with silicon tubes were surgically inserted into the air sacs.

Table 2. Experimental conditions.

Frequency (GHz)	2.45
Tx antenna gain (dB)	10.00
Tx power (dBW)	-40.00
EIRP (dBW)	-30.00
Free space pass loss (dB)	29.77
Reflection loss (dB)	3.00
Body attenuation (dB)	12.0
Rx Antenna gain (dB)	10.00
Antenna pointing loss	3.00
Receiving power (dBW)	-67.76
Noise temp of Receiver (K)	1200.00
Noise power density (dBW/Hz)	-197.81
G/T(dB/K)	-20.79
Bandwidth (4 kHz)	-36.02
C/No (dB Hz)	91.15
Required C/No (dB Hz)	50.40
Margin(dB)*	40.75

3.3. Experimental Results Pigeon

Respiration-induced changes in received power and heartbeat-synchronized waveforms were obtained from all target birds. Fig. 8 shows changes in the received magnitude waveform (top) and changes in the abdominal air sac pressure obtained by the pressure sensor, both of which are synchronous.

Similarly, the change in the received power obtained from the chest probe of the pigeon (*Columba livia*), the FFT of the signal, the inverse FFT of the frequency components below 17 Hz, and the differentiation of this waveform are shown in Fig. 9. The waveform and the electrocardiogram obtained at the same time are also shown.

A heartbeat is obtained from a chest probe. The measured signal was about 20 dB lower than the calculated value. The

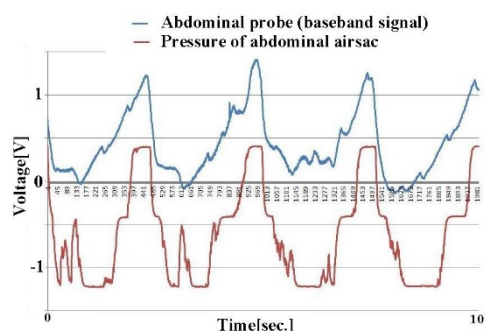


Fig. 8. Magnitude waveform from abdominal probe (top) and pressure of abdominal air sac (bottom) obtained with pressure sensor inserted into abdominal air sac.

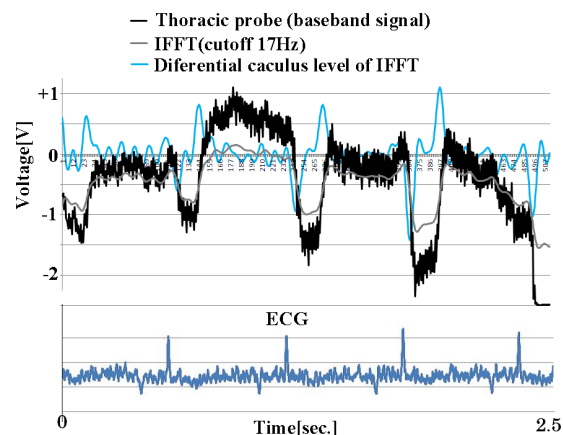


Fig. 9. Phase waveform (black) obtained from chest probe, its FFT, inverse FFT, and differentiated signal (synchronized with electrocardiogram R wave).

reason for this was clarified during the post-experiment autopsy. Homing pigeons used for racing have well-developed breast wall meat, which is not much different from chicken breast wall thickness, and their wing meat is thicker than that of chickens. Nevertheless, a margin of about 30 dB was secured.

3.4. Chicken

Eight chickens were viewed using a circularly polarized probe and compared with esophageal catheter data. In Fig. 10, photograph shows the measurements taken on chest side of chickens.

3.5. Evaluation of Magnitude Waveform for Chicken

The obtained magnitude waveform (black) is shown in Fig. 11. This waveform is strongly correlated with the anterior thoracic air sac pressure (yellow). In birds, the breathing pattern is inspiration, short duration, expiration, then long duration (one cycle) and both curves (black and yellow) suggest that principle. Amplitude modulation of the anterior thoracic air sac, indicated by asterisks, can be observed as turbulent airflow from other air sacs (posterior air sacs) to the precordial air sacs via the lungs. Such vibrations are due to phase differences in skeletal muscle contractures, which are described in detail in the paper [2]. Birds, unlike mammals, are efficient with more than one airflow to the lungs

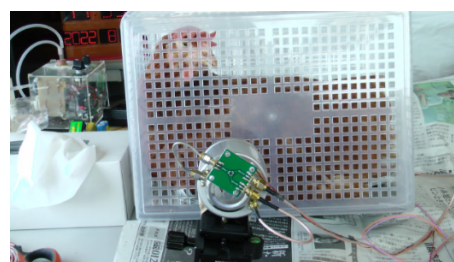


Fig. 10. Photograph of measurements taken on chest side of chickens (isoflurane anesthesia device shown on left).

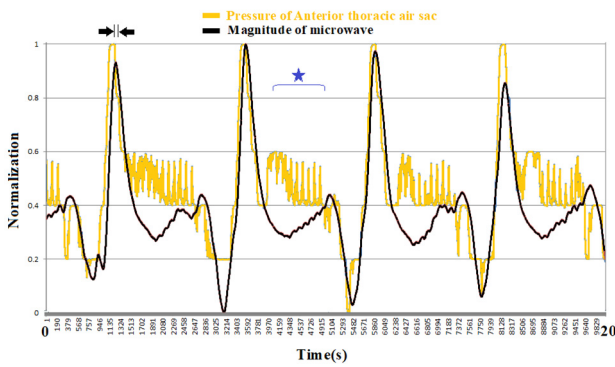


Fig. 11. Normalized waves of Magnitude of microwave and pressure of anterior thoracic air sac. During the asterisks, air flows with vibration are inserted from another air sacs via lungs.

per breath.

The magnitude waveform has a strong correlation with the anterior thoracic air sac pressure. It is speculated that the skeletal muscles that generate the anterior thoracic air sac pressure strongly affect the movement of the chicken's chest wall. In more detail, it can be inferred from this graph that the breathing control muscles are different between the star-marked time period and the time period of inspiration and expiration.

3.6. Evaluation of Phase Waveform for Chicken

Fig. 12 shows the phase waveform of the microwaves (purple). There is a notch in the middle of the mountain-shaped waveform, as indicated by an arrow. This notch is synchronized with the aortic valve closing sound from the heart sound (green).

The upper part of the graph shows the angular velocity of the axial rotation of the esophagus. Previous studies [3] have shown that its amplitude correlates with blood pressure.

When the measurement point was determined at the timing of breathing and the correlation between the amplitude

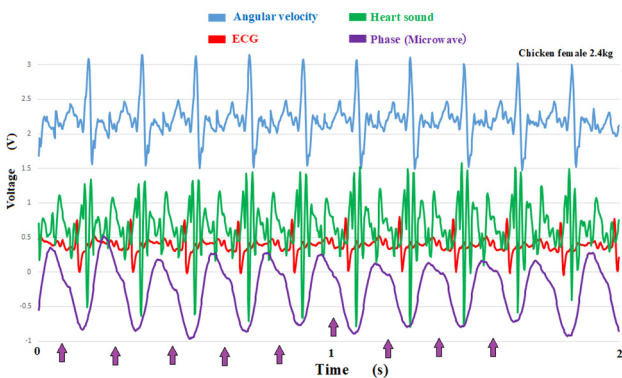


Fig. 12. Phase waveform for chicken (purple arrows indicate notches that occur at aortic valve closure; this timing can be deduced from heart sound).

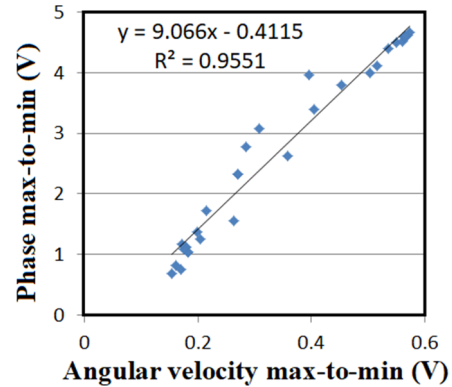


Fig. 13. Correlation between potential of angular velocity and potential of phase.

of the angular velocity and the amplitude of the microwave phase was obtained, a linear correlation was established at $R^2=0.95$ (Fig. 13).

This indicates that the microwave phase reflects the blood flow in the heart and that the notch measures the closing of the aortic valve and the subsequent inflow into the left atrium.

IV. CONSIDERATIONS

4.1. Comparison with Reflected Radar Doppler Method

Many experiments have been conducted on heartbeat/respiratory monitors using microwaves. We have developed a monitor that has a strong correlation between the cardiac output flow and the pressure of the anterior thoracic air sac in birds using transmission-type microwaves.

We can obtain not only the cardiac output flow but also the interval between beats (RR interval). This interval reflects the condition of autonomic nerves (sympathetic and parasympathetic nerve control) and is an important parameter for confirming health conditions. For radar Doppler, it is difficult to accurately measure interval fluctuations because increasing the frequency resolution leads to frequency components at intervals of Δt that are at least 1,024, 2,048, or more times the sampling time.

Therefore, the interval of time Δt becomes at least an error factor for time domain. Furthermore, since the RR interval evaluates the standard deviation of the 100 intervals, the error in Δt is included in the result of standard deviation. Therefore, the RR interval obtained from the heart rate by FFT using reflected radar Doppler is unreliable.

Since it is not fair to discuss only our strengths unilaterally, we will also introduce the advantages of the Doppler radar system. The biggest advantage is that only one antenna is required, so the high-frequency structure is extremely small. The distance setting range is also wide, so even if the target moves, it does not matter where it is within

Table 3. Comparison of reflective radar Doppler and proposed method.

	Radar Doppler	Transmission-type microwave
Frequency	10 GHz or more	L band, 2.4 GHz
RR interval	Inaccurate	Exact
Aortic valve notch	Not visible	Visible
Heartbeat	Indirect, Vibration of the chest wall	Direct monitor, obtain flow wave (blood pressure)
Application	Human	Birds, human

the line gain range. However, the target must be stationary at the moment of measurement [14-18]. To increase spatial resolution, increase the frequency. In this case, the penetration rate into the tissue decreases, so the distance should be shortened and the transmission power should be increased [19-20]. Furthermore, a detection method that emphasizes phase has been proposed to suppress magnitude wave due to respiration [21-22]. The paper [27] captures the waveform correlated with the blood flow with the reflection type, blood flow of intracranial space [7], and the paper [17] also reports the paper using the transmission microwave. A comparison of radar Doppler and the proposed method is given in Table 3 [14-26].

4.2. Future Outlook

Birds do not have a diaphragm and their lungs are hard and thus barely expand. They thus breathe by contracting balloon-like air sacs that expand in their chest and abdomen.

The avian great vessel is the right descending aorta. The cells of the left ventricle and the interventricular septum look morphologically abnormal. The muscle fibers are short and thick. The normal avian heart presents macro-histological abnormalities in macroscopic tissue sections. These abnormalities look similar to hypertrophic myocarditis in humans.

Cardiac ejection fraction is close to 100%, so the branch of the His bundle from the atrial node is running outside of left ventricular descends laterally rather than medially. The heart rate of chickens is 200–300 beats/min, Hummingbird has more than 1,000/min, which is much faster than that of humans. Birds cannot accurately transmit electrical stimulation to the left ventricle with the same conduction pathway as mammals. Therefore, the outside of the left ventricular wall is a stimulus conduction path (myocardium degenerated like a nerve fiber).

The autonomic nervous system is controlled by a battle between the sympathetic and parasympathetic nervous systems. The indices are the standard deviation of the RR

interval, systolic blood pressure, and heart rate. Parasympathetic nerves in birds are weakly suppressed and many birds suffer myocardial damage and large blood vessel damage when excited. Air sacs are controlled by the movement of respiratory muscles (skeletal muscles), but the subcutaneous tissue of birds has extremely weak connections and adhesions with the fascia, making it difficult to visually detect changes associated with respiration. Therefore, it is not possible to screen infected birds based on their appearance alone.

Infection in chickens with a highly pathogenic avian influenza virus propagates in type II alveolar epithelium and causes a cytokine storm. This leads to tachycardia, low blood pressure, shallow breathing, increased breathing rate, and slower skeletal muscle contraction. A diagnosis should be confirmed by a polymerase chain reaction test. However, at poultry farms, a simple antigen-antibody reaction is used. It takes time for the influenza virus antibody titer to reach a positive level. In settings with a lot of chickens, if the cardiac output and respiratory pattern of poultry could be monitored without restraint and contact, infected birds could be screened early and isolated from the population, preventing the culling of many birds.

The hosts of avian influenza viruses are mainly waterfowl such as ducks and swans, not chickens. A low-virulence influenza virus replicates slowly in the gut rather than the lungs, with a potential prevalence of up to 30% in nature. In poultry, on the other hand, the influenza virus has been found to spread rapidly from the intestine to the lungs, and it has been reported that even low pathogenicity causes mild respiratory symptoms. Screening for early mild respiratory distress is therefore important in the poultry industry. We recommend a system that can continuously monitor cardiac output and breathing patterns without contact.

V. CONCLUSION

We developed a device that can monitor the cardiac output and anterior thoracic air sac pressure in birds using transmission-type microwaves (2.4–2.5 GHz). Compared to reflector-type radar Doppler devices, the proposed device can visualize blood flow and continuously measure breathing patterns that are correlated with the anterior thoracic air sac pressure. Data collection allows the early screening of unwell birds, which can be isolated to prevent mass infections in poultry houses and prevent pandemics.

ACKNOWLEDGMENTS

The intellectual property rights of the equipment used in this research are owned by Tasada Works Inc. in Takaoka City, Toyama Prefecture (President: Mr. Masuhisa Ta). We

would like to thank Dr. Kaoru Nakata, Ms. Noriko Numata, and Ms. Miyoshi Tanaka of the Tokai University School of Medicine, and Mr. Kokuryo Mitsuhashi and Ms. Megumi Amano of Seisa University for their assistance in the experiment. Pigeons (racing pigeons) were obtained courtesy of Yamazaki Pigeon (Mr. Kiyoshi Yamazaki) in Ueda City. Regarding chicken acquisition, we would like to thank Mr. Masatake Kamata (Takaoka Hikarien Poultry Farm), Veterinary Doctor Hisayoshi Nakamura (Takaoka City), Mr. Shigeru Yamamoto (Takaoka City), and Ms. Hideko Nagahara (Dog Friends) for their excellent support. Dr. Kiyooki Ozaki and Mr. Noboru Nakamura from the Yamashina Institute for Ornithology provided guidance and suggestions.

Since 2012, this study has been submitted the Tokai University `Animal Experiment Plan and has undergone appropriate review. This research was funded by grants-in-aid for scientific research (grants 21241042, 23651169, 24241058, 26630165, and 15H01791) from the Ministry of Education, Culture, Sports, Science and Technology. The authors have no conflicts of interest to declare.

Every year, we have submitted experiment plans to Tokai University based on the regulations of the Japanese Ministry of Health, Labor and Welfare and the Ministry of the Environment on experimental animals, which were reviewed and approved by an expert committee. The themes covered in these applications are “Acquisition of avian physiological digital data, including anesthesia, surgical procedures, and insert electronic devices, also including free space flight data collections of crow, pheasant, and pigeon with electronic devices.”(Table 4).

Table 4. Approval number and target birds related to this experiment (FY-2013-2022 Tokai University, Japan).

Year	Approval number	Target animal
FY-2011	111114	Chicken
	111115	Quail
	111117	Crow
FY2012	111114 continued	Chicken
	122020	Chicken
	122021	Quail
	122022	Crow
	121083	Pheasant
	121111	*
FY-2013	133009	Chicken
	133007	Quail
	133008	Crow
	132036	*
FY-2014	144009	Chicken
	141007	Pheasant
	141006	Crow

Table 4. Continued.

Year	Approval number	Target animal
FY-2015	151021	Chicken
	151022	Pheasant
	151023	Crow
	151077	Pigeon
FY-2016	162049	Chicken
	162050	Pigeon
	162027	Pheasant
	162048	Crow
	16081	Pigeon+
FY-2017	172032	Pigeon+
	173034	Crow
	173027	Chicken
	173028	Pigeon
	173032	Pheasant
FY-2018	184019	Pigeon
	184020	Pheasant
	183013	Pigeon+
	184039	Chicken+
	184040	Crow
FY2019	195020	Chicken
	195021	Pigeon
	194017	Pigeon+
	1950027	Crow
FY-2020	201053	Crow
	201054	Chicken
FY-2021	211055	Chicken
FY-2022	221073	Chicken

*: Verification of prototype portable inhalation anesthesia device.
 +: Verification of airflow between air sacs with special electronic device.

REFERENCES

- [1] K. Nakada and J. Hata, "Development and physiological assessments of multimedia avian esophageal catheter system," *Journal of Multimedia Information System*, vol. 5, no. 2, pp.121-130, 2018.
- [2] I. Nakajima, S. Tanaka, K. Mitsuhashi, J. Hata, and T. Nakajima, "Detecting of periodic fasciculations of avian muscles using magnetic and other multimedia devices," *Journal of Multimedia Information System*, vol. 6, no. 4, pp. 293-302, 2019.
- [3] I. Nakajima, I. Kuwahira, S. Hori, and K. Mitsuhashi1, "Correlation of axillary artery pressure and phase of esophageal impedance in chickens," *Jourmanl of Multimedia Information System*, vol. 9, no. 2, pp. 161-172,

- 2022.
- [4] L. Gun, D. Ning, and Z. Liang, "Effective permittivity of biological tissue: Comparison of theoretical model and experiment," *Journal Mathematical Problems in Engineering*, vol. 2017, p. 7249672.
- [5] J. Leroy, C. Dalmay, A. Landoulsi, F. Hjeij, C. Melin, and B. Besette, et al., "Microfluidic biosensors for microwave dielectric spectroscopy," *Sensors and Actuators, A: Physical*, vol. 229, pp. 172-181, 2015.
- [6] F. Farsaci, E. Tellone, M. Cavallaro, A. Russo, and S. Ficarra, "Low frequency dielectric characteristics of human blood: A non-equilibrium thermodynamic approach," *Journal of Molecular Liquids*, vol. 188, pp. 113-119, 2013.
- [7] G. Li and X. F. Pang, "Effects of electromagnetic field exposure on electromagnetic properties of biological tissues," *Progress in Biochemistry and Biophysics*, vol. 38, no. 7, pp. 604-610, 2011.
- [8] E. Marzec and W. Warchoł, "Dielectric properties of a protein-water system in selected animal tissues," *Bioelectrochemistry*, vol. 65, no. 2, pp. 89-94, 2005.
- [9] E. Marzec, P. Sosnowski, J. Olszewski, H. Krauss, K. Bahloul, and W. Samborski, et al., "Dielectric relaxation of normothermic and hypothermic rat corneas," *Bioelectrochemistry*, vol. 101, pp. 132-137, 2015.
- [10] T. Dai and A. Adler, "In vivo blood characterization from bioimpedance spectroscopy of blood pooling," *IEEE Transactions on Instrumentation and Measurement*, vol. 58, no. 11, pp. 3831-3838, 2009.
- [11] Y. Otaki, Y. Ebana, S. Yoshikawa, and M. Isobe, "Dielectric permittivity change detects the process of blood coagulation: Comparative study of dielectric coagulometry with rotational thromboelastometry," *Thrombosis Research*, vol. 145, pp. 3-11, 2016.
- [12] Y. Llave, K. Mori, D. Kambayashi, M. Fukuoka, and N. Sakai, "Dielectric properties and model food application of tylose water pastes during microwave thawing and heating," *Journal of Food Engineering*, 2015.
- [13] N. Simicevic and D. T. Haynie, "FDTD simulation of exposure of biological material to electromagnetic nanopulses," *Physics in Medicine and Biology*, vol. 50, no. 2, pp. 347-360, 2005.
- [14] W. J. K. Raymond, C. K. Chakrabarty, G. C. Hock, and A. B. Ghani, "Complex permittivity measurement using capacitance method from 300 kHz to 50 MHz," *Measurement*, vol. 46, no. 10, pp. 3796-3801, 2013.
- [15] H. F. Cook, "A comparison of the dielectric behaviour of pure water and human blood at microwave frequencies," *British Journal of Applied Physics*, vol. 3, no. 8, article 302, pp. 249-255, 1952.
- [16] M. Aweda, R. Meindinyo, S. Gbenebitse, and A. Z. Ibitoye, "Microwave radiation exposures affect cardiovascular system and antioxidants modify the effects," *Pelagia Research Library Advances in Applied Science Research*, vol. 2, no. 2, pp. 246-251, 2011.
- [17] H. Tan, D. Qiao, and Y. Li, "Non-contact heart rate tracking using Doppler radar," in *Proceedings of the 2012 International Conference on Systems and Informatics (ICSAI2012)*, 2012, pp. 1711-1714.
- [18] M. Alizadeh, G. Shaker, and S. Safavi-Naeini, "Remote heart rate sensing with mm-wave radar," in *Proceedings of the 2018 18th International Symposium on Antenna Technology and Applied Electromagnetics (ANTEM)*, 2018, pp. 1-2.
- [19] D. Obeid, S. Sadek, G. Zaharia, and G. E. Zein, "Doppler radar for heartbeat rate and heart rate variability extraction," in *Proceedings of the 2011 E-Health and Bioengineering Conference (EHB)*, 2011.
- [20] V. Petrović, M. Janković, A. Lupšić, V. Mihajlović, and J. Popović-Božović, "High-accuracy real-time monitoring of heart rate variability using 24 GHz continuous-wave doppler radar," *IEEE Access*, 2019, vol. 7, pp. 74721-74733.
- [21] P. Zhao, C. X. Lu, B. Wang, C. Chen, L. Xie, and M. Wang, "Heart rate sensing with a robot mounted mmwave radar," in *Proceedings of the 2020 IEEE International Conference on Robotics and Automation (ICRA)*, 2020, pp. 2812-2818.
- [22] K. Z. Li and W. Z. Zhu, "Research on non-contact respiration and heart rate monitoring algorithm based on 77G FMCW radar," in *Proceedings of the 2022 2nd International Conference on Consumer Electronics and Computer Engineering (ICCECE)*, 2022, pp. 915-920.
- [23] K. Higashi, G. Sun, and K. Ishibashi, "Precise heart rate measurement using non-contact Doppler radar assisted by machine-learning-based sleep posture estimation," in *Proceedings of the 2019 41st Annual International Conference of the IEEE Engineering in Medicine and Biology Society (EMBC)*, 2019, pp. 788-791.
- [24] L. Ren, H. Wang, K. Naishadham, O. Kilic, and A. E. Fathy, "Phase-based methods for heart rate detection using UWB impulse Doppler radar," *IEEE Transactions on Microwave Theory and Techniques*, 2016, vol. 64, no. 10, pp. 3319-3331.
- [25] A. Mase, Y. Kogi, and T. Maruyama, "Real-time evaluation of heart rate and heart rate variability using microwave reflectometry," in *Proceedings of the 2018 IEEE International Microwave Biomedical Conference (IMBioC)*, 2018, pp. 160-162.
- [26] T. Lauteslager, M. Tommer, K. G. Kjølgaard, T. S. Lande, and T. G. Constandinou, "Intracranial heart rate

detection using UWB radar," in *Proceedings of the 2016 IEEE Biomedical Circuits and Systems Conference (BioCAS)*, 2016, pp. 119-122.

- [27] J. Sato, K. Kishimoto, N. Honma, M. Iwai, and K. Kobayashi, "Correlation between microwave and blood pressure response waveforms", in *2018 International Symposium on Antennas and Propagation (ISAP)*, 2018, pp. 1-2.
- [28] P. F. Battley, *Contrasting Extreme Long-Distance Migration Patterns in Bar-Tailed Godwits Limosa lapponica*, 2012. https://www.researchgate.net/figure/Tracks-of-satellite-tagged-bar-tailed-godwits-on-southward-migration-with-place-names_fig1_263574008.

AUTHORS



Isao Nakajima He is a specially appointed professor of Seisa University and a visiting professor of Nakajima Labo. at the Dept. of Emergency Medicine and Critical Care, Tokai University School of Medicine. He got the Doctor of Applied Informatics (Ph.D.), Graduate School of Applied Informatics University of Hyogo 2009, and the Doctor of Medicine (Ph.D.), Post Graduate School of Medical Science Tokai University 1988, and the Medical Doctor (M.D.) from Tokai University School of Medicine 1980. He has been aiming to send huge multimedia data from moving ambulance via communications satellite to assist patient's critical condition. He is a board member of the Pacific Science Congress, a Rapporteur for eHealth of ITU-D SG2 (2014-2021), and a specially appointed researcher at the Yamashina Institute for Ornithology, Japan.



Ichiro Kuwahira He has received his MD degree from Tokai University School of Medicine, Kanagawa, in 1980. In 1984, he received a PhD degree in Tokai University Graduate School of Medicine. Since then, he has been mainly involved in respiratory medicine and physiology. He was appointed to a professor of medicine, Tokai University School of Medicine in 2005, and to a specially-appointed professor in 2020. He acted as a hospital director of Tokai University Tokyo Hospital from 2004 to 2011.



Jun-ichi Hata He has received his MD degree from Keio University School of Medicine, Tokyo, in 1966. In 1971, he received a PhD degree in Keio University Post Graduate School of Medicine. Since then, he has been mainly involved in molecular pathology for pediatric tumors and embryonal pathology. He was appointed to a professor of pathology, Keio University School of Medicine in 1990. In 2013, he has been appointed as research director of Central Institute for Experimental Animals.

